

COMBINED VOLTAGE ORIENTED CONTROL AND DIRECT POWER CONTROL BASED ON BACKSTEPPING CONTROL FOR FOUR-LEG PWM RECTIFIER UNDER UNBALANCED CONDITIONS

Chebabhi Ali¹–Barkat Said¹–Abdelhalim Kessal^{2*}

¹EE Laboratory, Electrical Engineering Department, Faculty of Technology, University of Msila, Algeria.

²LPMRN Laboratory, Faculty of Sciences and Technology, University of Bordj Bou Arreridj, Algeria.

ARTICLE INFO

Article history:

Received: 05.10.2020.

Received in revised form: 30.05.2021.

Accepted: 31.05.2021.

Keywords:

Four-leg PWM rectifier

Voltage-oriented control and direct power control (VOC-DPC) method

Synchronous rotating frame (dq0-frame)

Backstepping control (BSC)

Power quality and robustness

DOI: <https://doi.org/10.30765/er.2020>

Abstract:

The present paper proposes a combined voltage-oriented control and direct power control (VOC-DPC) method associated with the backstepping control technique for a three-phase four-wire grid-connected four-leg rectifier in the synchronous rotating frame without using phase locked loop (PLL) and Parks transformation under balanced and unbalanced load and grid conditions. This control method is proposed in order to remove the drawbacks of the conventional VOC based on the PLL technique. The proposed control method is able to enhance the control performance and dynamic responses of the system when considering slow dynamics and instability issues of the PLL in several cases and can decrease the computational burden due to the absence of PLL and Park transformation. In addition, the performance of the proposed VOC-DPC method is enhanced by using backstepping control (BSC) based on Lyabonov theory for both the input currents and DC-bus voltage loops. As a consequence, constant DC-bus voltage, unit power factor, sinusoidal input currents, and neutral current minimization can be accurately carried out under both DC-bus voltage and load variations. Furthermore, robustness against filter inductance variations can also be achieved. The effectiveness, superiority, and performance of the proposed control method for a four-leg rectifier based on BSC in the dq0-frame are validated by several processor-in-the-loop (PIL) co-simulation tests using the STM32F407 discovery development board.

1 Introduction

In recent years, three-phase four-leg PWM converters have become much more popular and widely used in many recent power applications, such as renewable energy-based grid-connected and stand-alone power generation systems [1] - [3], active front-end PWM rectifiers, active filters (AF), distributed static compensators (DSTATCOM) [4] - [6], electric machines [7], and electric vehicle (EV) charging systems [8]. Because of their superior input current waveforms with lower THD, high DC-bus voltage utilization, controllable DC-bus voltage, and bidirectional power flow, they are regarded as highly efficient devices for high-power applications. Moreover, these converters, including four-leg PWM rectifiers, have the capability to provide a zero-sequence input current path and control and are appropriate to maintain symmetrical sinusoidal grid currents and voltages under all loading and grid conditions, including unbalanced single-phase load [4], [7], which can significantly decrease the grid power quality or even cause stability problems.

The two most common control strategies for these converters are the traditional voltage-oriented control (VOC) method and direct power control (DPC) method. Compared to the DPC method, the traditional VOC

* Corresponding author

E-mail address: abdelhalim.kessal@univ-bba.dz

method in the synchronous rotating frame (dq0-frame) has been widely utilized thanks to its simple structure and ease of implementation. This provides a time-invariant four-leg PWM converter mathematical model in the dq0-frame, which can be controlled readily using diverse controllers. The grid-synchronization-method and Park's transformation are two highly significant parts of this control method and are used for precisely deriving the system dq0 time-invariant model and synchronizing the converter to the grid. The synchronization-method has a significant role in VOC method, since it is used to extract the grid voltage phase angle utilized in diverse Park's and inverse Park's transformations and consequently providing the accuracy of current control in the dq0-frame for four-leg PWM converters [9], [10]. So far, the phase-locked loop (PLL) has been the most widely used to extract the phase-angle in the traditional VOC method, providing high control dynamics when the grid voltage phase-angle is correctly detected [11]. However, the slow dynamics of the PLL increases the difficulty of grid voltage frequency or phase-angle detection, which will affect the VOC control performance and dynamics responses of the grid-connected converter system as well. Moreover, the PLL larger bandwidth and the parameters of its PI closed-loop control may cause an unstable phenomenon when subjected to distortion and unbalanced grid voltage conditions, which makes the high-frequency resonance more probable to occur due to a smaller phase margin [11], [12]. Furthermore, the inherent complexity of the PLL and the various Parks transformations, as well as their inverse use in this control method, adds a high computational burden [13]. In addition, it is well known that the grid voltage distortion and unbalanced events impact the accuracy and performance of this PLL, which adversely impacts the traditional VOC performance and dynamic responses of the grid-connected PWM rectifier system [14].

To remedy the aforementioned problems with high control performance and lower computational burden under voltage distortion and unbalanced conditions, several current control methods in the dq-frame without synchronization method and Park transformation have been proposed in recent literature. These methods include combined VOC and DPC (VOC-DPC) method in dq-frame based on instantaneous power method concepts [15], [16] and nonlinear observed grid-phase based VOC method [17].

Among the abovementioned control methods, the combined VOC-DPC method outperforms the others in terms of control performance, dynamic responses, computational burden, and ease of implementation. The concept of this method is to determine the rectifier input current in the dq-frame using the instantaneous power method concept and balanced grid voltage condition, which is not only used for controlling the grid-connected PWM converters but also to provide the model of three-phase grid-connected PWM converters in the dq-frame (a linear time-invariant system in the dq-frame) based on the instantaneous active and reactive power theory without using PLL and Parks transformation, which combines the advantages of traditional VOC and DPC and has the same properties and control circuit structure as the traditional VOC when the grid voltage phase angle is correctly detected. However, when the outer DC-bus voltage control loop and the inner current controller loops of this control method are achieved using traditional proportional integral (PI) controllers, the inherent nonlinearities of the four-wire grid-connected four-leg rectifiers and undesirable perturbations due to parameter variations will not only impact the performance and stability of the traditional PI controllers [15], but also lead to poor dynamic responses in transient and steady states.

In order to further improve transient and steady-state control performance and provide high robustness to parameter variations in three-phase, grid-connected four-leg PWM converters, numerous control approaches based on the VOC method have been suggested in recent years. These techniques include sliding mode control (SMC) [18], [19], fuzzy logic control (FLC) [20], and backstepping control (NBSC) [5], [21], [22].

Among these control techniques, backstepping control (BSC) is found to be an appropriate and effective technique for PWM converter control processes due to the inherent advantages of systematic, recursive controller design based on the Lyapunov function, which insures asymptotic tracking error convergence in all loops, successful robustness against parameter variations and uncertainty rejection, ease in practical implementation, and beneficial performance under various operating conditions. Since the model of the PWM rectifier can be represented as a linear time-invariant system in the dq0-frame, the BSC technique can be directly used on the outer and inner loops. In [23] - [26], researchers have proposed a BSC for a three-phase, three-leg PWM rectifier, and the results show that the BSC has high control performance and dynamic responses in transient and steady states in terms of harmonic suppression, power factor correction, reactive power compensation, stability, and robustness against parameter variations. However, in the aforementioned works, the three-leg PWM rectifier is considered as the main converter. Consequently, zero-sequence current generated in the case of single-phase unbalanced loads connected to the main grid or under unbalanced grid

voltages is not taken into consideration, and the stability and control performance of the grid-connected four-leg PWM rectifier cannot be ensured under these unbalanced conditions.

To address the aforesaid problems, a VOC-DPC method based on BSC is proposed in this paper to control a three-phase four-leg rectifier. The main contributions of this work are listed as follows:

1. A four-leg rectifier configuration is used because it provides a zero-sequence current channel and control to avoid PCC voltage fluctuations.
2. An improved VOC-DPC method is proposed to eliminate the impact of PLL and Park transformation on the traditional VOC method, which reduces the computational burden and improves the control performance under all conduction. The active and reactive input currents, as well as the input voltage references, are determined in the stationary frame using both VOC and DPC concepts, without the use of PLL or Park transformation.
3. In the outer and inner loops of the proposed VOC-DPC method, BSC is suggested to control the input currents in the dq0-frame and DC-bus voltage. The use of BSC instead of the traditional PI controller allows zero steady-state tracking errors for the input currents and DC-bus voltage, suppression of grid current harmonics, unity power factor (UPF), and zero-sequence current elimination.

In this work, the transient and steady state performances of the proposed VOC-DPC-BSC control based grid-connected four-leg rectifier are evaluated and compared with those of the VOC-DPC based on the traditional PI -controller (VOC-DPC-PIC) in terms of trajectory tracking, DC-bus voltage oscillation and stabilization, reactive power compensation, input current harmonic mitigation, power factor correction, zero-sequence current elimination, and robustness against filter inductor variations.

The proposed method VOC-DPC with a BSC shows satisfactory results for all the previous performance indicators, which demonstrates the superiority and effectiveness of the proposed control method.

This paper is organized as follows: the modelling of the three-phase PWM rectifier in the dq0-frame on the basis of DPC concepts is presented in Section 2. Section 3 presents the proposed VOC-DPC method based on BSC, whereas the BSC used in the outer and inner loops is described in Section 4. The results of PIL co-simulations and the discussions on the proposed VOC-DPC based on BSC and PI are presented in Section 5, and finally, some conclusions on this study are drawn in Section 6.

2 Three-phase four-wire grid-connected four-leg PWM rectifier modelling

Fig. 1 illustrates the three-phase four-leg PWM rectifier topology connected to four-wire grid at the point of common coupling (PCC) through filter inductances (L_{fabcn}) with internal resistances (R_{fabcn}). In this figure, i_{fabcn} and v_{fabcn} represent the four-leg rectifier input currents and voltages, respectively. i_{gabcn} and v_{gabcn} denote the PCC currents and voltages, respectively. e_{abc} are the grid sinusoidal voltages. The output DC-bus voltage, output DC current, capacitor current, and load current are denoted as V_{dc} , I_{dc} , I_c , and I_L , respectively. The DC-bus capacitor and load are identified as C_{dc} and R_L , respectively.

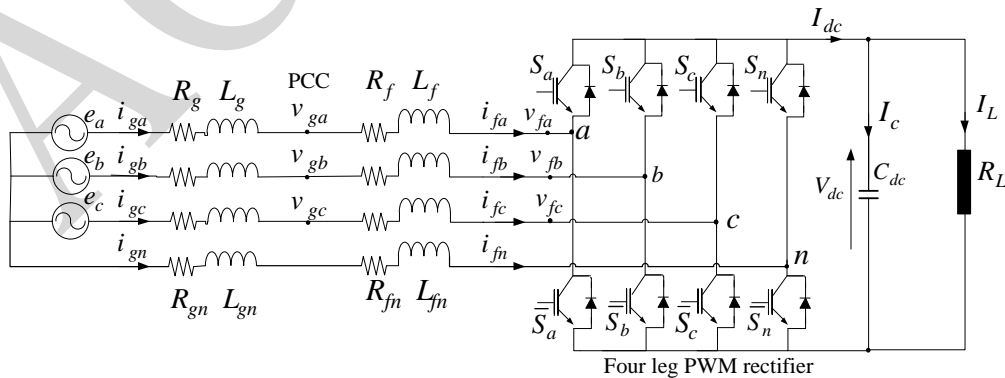


Figure 1. Power circuit of three phase grid-connected four-leg rectifier.

The dynamic equations describing the input currents and the DC-bus voltage of the three-phase four-leg rectifier shown in Fig. 1 can be given in the abc reference frame as follows:

$$\begin{cases} L_{fa} \frac{di_{fa}}{dt} = v_{ga} - R_{fa} i_{fa} - v_{fa} + R_{fn} i_{fn} + L_{fn} \frac{di_{fn}}{dt} \\ L_{fb} \frac{di_{fb}}{dt} = v_{gb} - R_{fb} i_{fb} - v_{fb} + R_{fn} i_{fn} + L_{fn} \frac{di_{fn}}{dt} \\ L_{fc} \frac{di_{fc}}{dt} = v_{gc} - R_{fc} i_{fc} - v_{fc} + R_{fn} i_{fn} + L_{fn} \frac{di_{fn}}{dt} \\ C_{dc} \frac{dV_{dc}}{dt} = (S_a i_{fa} + S_b i_{fb} + S_c i_{fc} + S_n i_{fn}) - I_L \end{cases} \quad (1)$$

where S_a , S_b , S_c , and S_n are the switching states of the rectifier power switches. The neutral phase input current i_{fn} is given as:

$$i_{fa} + i_{fb} + i_{fc} = -i_{fn} \quad (2)$$

From this equation, the zero-sequence input current i_{f0} is computed as:

$$i_{f0} = \frac{1}{\sqrt{3}} (i_{fa} + i_{fb} + i_{fc}) = -\frac{1}{\sqrt{3}} i_{fn} \quad (3)$$

The input voltages and the DC-bus voltage of the three-phase four-leg rectifier can be derived in the dq0-frame using instantaneous grid active and reactive power theory without need for Park transformation as follows [15]:

$$\begin{cases} v_{fd} = v_{gd} - L_f \frac{di_{fd}}{dt} - R_f i_{fd} + L_f \omega i_{fq} \\ v_{fq} = v_{gq} - L_f \frac{di_{fq}}{dt} - R_f i_{fq} - L_f \omega i_{fd} \\ v_{f0} = v_{g0} - (L_f + 3L_n) \frac{di_{f0}}{dt} - (R_f + 3L_n) i_{f0} \\ C_{dc} \frac{dV_{dc}}{dt} = (S_d i_{fd} + S_q i_{fq} + S_0 i_{f0}) - I_L \end{cases} \quad (4)$$

where, v_{fdq0} and i_{fdq0} stand for the input currents and voltages of the four-leg rectifier in the dq0-frame, respectively. S_d , S_q , and S_0 are the switching states in the dq0-frame, and ω is the PCC angular-frequency.

The dynamics of input currents and DC-bus voltage in the dq0-frame are given by applying the grid voltage orientation concept when the d-axis grid voltage v_{gd} is oriented with the grid voltage vector and the q-axis grid voltage v_{gq} is in quadrature with it ($v_{gd}=V_{gmax}$, $v_{gq}=v_{g0}=0$, where V_{gmax} is the grid voltage) as follows:

$$\begin{cases} \frac{di_{fd}}{dt} = -\frac{R_f}{L_f} i_{fd} + \omega i_{fq} + \frac{v_{gd}}{L_f} - \frac{v_{fd}}{L_f} \\ \frac{di_{fq}}{dt} = -\frac{R_f}{L_f} i_{fq} - \omega i_{fd} - \frac{v_{fq}}{L_f} \\ \frac{di_{f0}}{dt} = -\frac{(R_f + 3R_n)}{(L_f + 3L_n)} i_{f0} - \frac{v_{f0}}{(L_f + 3L_n)} \\ \frac{dV_{dc}}{dt} = \frac{1}{C_{dc}} (I_{dc} - I_L) = \frac{v_{gd}}{C_{dc} V_{dc}} i_{fd} - \frac{V_{dc}}{C_{dc} R_L} \end{cases} \quad (5)$$

Equation (5) reveal a coupling effect between input currents i_{fd} and i_{fq} . Therefore, the following control variables u_d , u_q , u_0 , and u_{dc} are introduced into Eq. (6) to reduce this coupling effect and enable decoupling control between the input currents in the following manner:

$$\begin{cases} u_d = L_f \frac{di_{fd}}{dt} + R_f i_{fd} \\ u_q = L_f \frac{di_{fq}}{dt} + R_f i_{fq} \\ u_0 = (L_f + 3L_n) \frac{di_{f0}}{dt} + (R_f + 3R_n) i_{f0} \\ u_{dc} = i_{fd} = \frac{C_{dc} V_{dc}}{v_{gd}} \left(\frac{dV_{dc}}{dt} + \frac{V_{dc}}{C_{dc} R_L} \right) \end{cases} \quad (6)$$

The rectifier input voltages v_{fq0} and d-axis input current i_{fd} are given by putting (6) into (5) as follows:

$$\begin{cases} v_{fd} = -u_d + L_f \omega i_{fq} + v_{gd} \\ v_{fq} = -u_q - L_f \omega i_{fd} \\ v_{f0} = -u_0 \\ i_{fd} = \frac{C_{dc} V_{dc}}{v_{gd}} \left(\frac{dV_{dc}}{dt} + \frac{V_{dc}}{C_{dc} R_L} \right) \end{cases} \quad (7)$$

According to (7), the input currents i_{fd} and i_{fq} can be independently controlled by the decoupling control variables u_d and u_q .

3 Proposed combined VOC-DPC method based on BSC technique

The suggested VOC-DPC method with BSC technique for the four-wire grid-connected four-leg PWM rectifier in dq0-frame is depicted in Fig. 3. The suggested method is founded on both the VOC and DPC concepts; the input voltage references in the dq0-frame v_{fdq0}^* are provided based on the VOC concept using the proposed BSC of the input currents in the inner loops. The d-axis input current reference is provided by the DC-bus voltage loop that ensures the input current control and zero sequence current elimination. On the other hand, the input currents i_{fdq0} in the dq0-frame used in the inner loop and the input voltage references in the $\alpha\beta 0$ -frame $v_{f\alpha\beta 0}^*$ required by the 3DSVPWM method are derived based on the DPC concept using Eqs. (17) or (32).

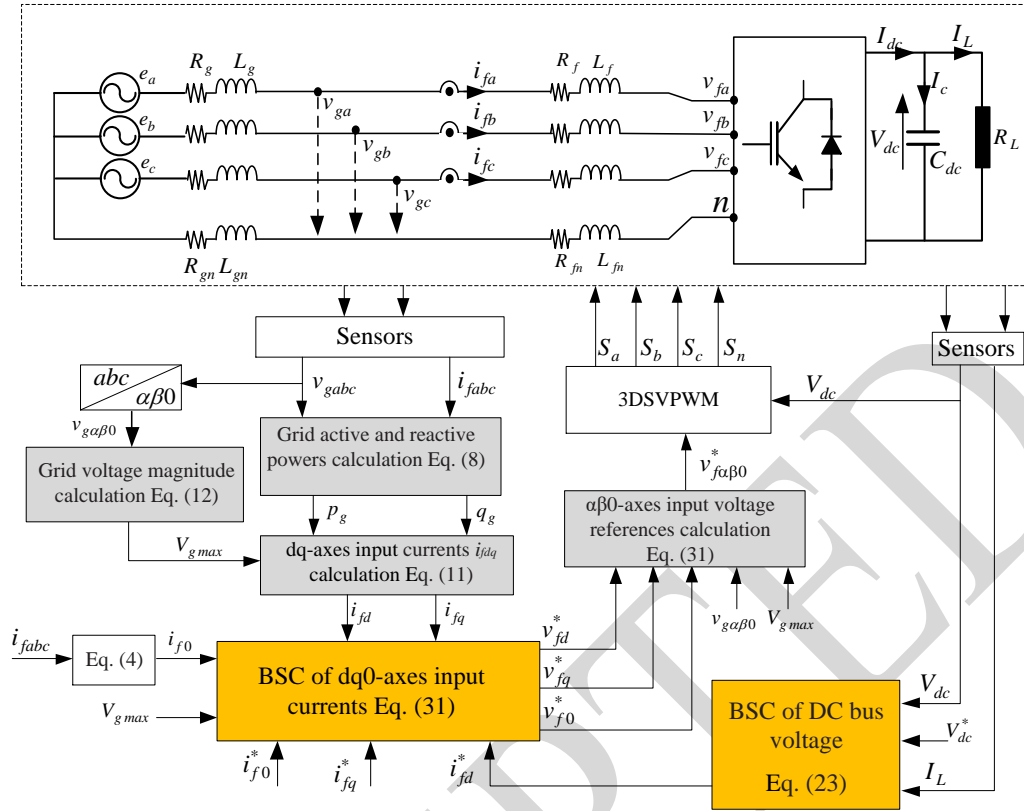


Figure 2. Block diagram of the proposed VOC-DPC with BSC of the three-phase four-wire grid-connected four-leg PWM rectifier.

According to the instantaneous power theory [27], [28], the grid active and reactive powers (p_g and q_g) can be calculated in the three phase (abc) reference frame as follows:

$$\begin{cases} p_g = v_{ga}i_{fa} + v_{gb}i_{fb} + v_{gc}i_{fc} \\ q_g = \sqrt{\frac{1}{3}}[(v_{gb} - v_{gc})i_{fa} - (v_{gc} - v_{ga})i_{fb} + (v_{ga} - v_{gb})i_{fc}] \end{cases} \quad (8)$$

These grid powers can be calculated in the dq-frame as follows [27]:

$$\begin{cases} p_g = v_{gd}i_{fd} + v_{fq}i_{fq} \\ q_g = v_{gd}i_{fq} - v_{fq}i_{fd} \end{cases} \quad (9)$$

Applying the grid voltage orientation concept, the grid active and reactive powers in (9) becomes:

$$\begin{cases} p_g = V_{gmax}i_{fd} \\ q_g = V_{gmax}i_{fq} \end{cases} \quad (10)$$

Substituting (10) into (8), the input currents i_{fdq0} are expressed in the dq0-frame as functions of the three phase grid voltages, input currents, and the grid voltage magnitude as follows:

$$\begin{cases} i_{fd} = \frac{1}{V_{gmax}}(v_{ga}i_{fa} + v_{gb}i_{fb} + v_{gc}i_{fc}) \\ i_{fq} = \frac{1}{V_{gmax}\sqrt{3}}[(v_{gb} - v_{gc})i_{fa} - (v_{gc} - v_{ga})i_{fb} + (v_{ga} - v_{gb})i_{fc}] \end{cases} \quad (11)$$

The grid voltage magnitude can be expressed in the $\alpha\beta 0$ -frame as follows:

$$V_{gmax} = \sqrt{v_{g\alpha}^2 + v_{g\beta}^2} \quad (12)$$

By assuming that the grid voltages are balanced, these voltages in the $\alpha\beta 0$ -frame can be expressed as:

$$\begin{cases} v_{g\alpha} = V_{gmax} \cos(\omega t) \\ v_{g\beta} = V_{gmax} \sin(\omega t) \end{cases} \quad (13)$$

In the $\alpha\beta 0$ -frame, by multiplying simultaneously the input voltages v_{fa} and v_{fb} by the grid voltages v_{ga} and $v_{g\beta}$, it yields [28]:

$$\begin{cases} v_p = v_{g\alpha}v_{fa} + v_{g\beta}v_{fb} \\ v_q = v_{g\beta}v_{fa} - v_{g\alpha}v_{fb} \\ v_0 = v_{g0} = v_{f0} \end{cases} \quad (14)$$

where v_p and v_q are new variables used to simplify determining the input voltages v_{fa} and v_{fb} in the $\alpha\beta 0$ -frame from the dq0-frame without using the Park transformation [16].

Substituting (13) into (14), the new variables v_p , v_q and v_0 become:

$$\begin{bmatrix} v_p \\ v_q \\ v_0 \end{bmatrix} = V_{gmax} \begin{bmatrix} \cos(\omega t) & \sin(\omega t) & 0 \\ \sin(\omega t) & -\cos(\omega t) & 0 \\ 0 & 0 & 1 \end{bmatrix} \begin{bmatrix} v_{fa} \\ v_{fb} \\ v_{f0} \end{bmatrix} = V_{gmax} \begin{bmatrix} v_{fd} \\ v_{fq} \\ v_{f0} \end{bmatrix} \quad (15)$$

According to (15), the input voltages v_{fa} and v_{fb} in the dq0-frame are given as functions of the input voltages in the $\alpha\beta 0$ -frame v_{fa} and v_{fb} as follows:

$$\begin{bmatrix} v_{fd} \\ v_{fq} \\ v_{f0} \end{bmatrix} = \begin{bmatrix} \cos(\omega t) & \sin(\omega t) & 0 \\ \sin(\omega t) & -\cos(\omega t) & 0 \\ 0 & 0 & 1 \end{bmatrix} \begin{bmatrix} v_{fa} \\ v_{fb} \\ v_{f0} \end{bmatrix} \quad (16)$$

The input voltages v_{fa} , v_{fb} , and v_{f0} are derived from v_{fd} , v_{fq} , and v_{f0} without using Park transformation by substituting (13) into the inverse of (16) as follows:

$$\begin{bmatrix} v_{fa} \\ v_{fb} \\ v_{f0} \end{bmatrix} = \frac{1}{V_{gmax}} \begin{bmatrix} v_{g\alpha} & v_{g\beta} & 0 \\ v_{g\beta} & -v_{g\alpha} & 0 \\ 0 & 0 & 1 \end{bmatrix} \begin{bmatrix} v_{fd} \\ v_{fq} \\ v_{f0} \end{bmatrix} \quad (17)$$

This equation is used to provide the input voltage references $v_{f\alpha\beta 0}^*$ in the $\alpha\beta 0$ -frame required by the 3DSVPWM method from the input voltage references in the $dq 0$ -frame $v_{fdq 0}^*$ provided by the proposed BSC of the input currents and DC-bus voltage designed in the following subsection.

4 Proposed BSC for DC-bus voltage and input currents loops

In this subsection, the design of DC-bus voltage and input currents backstepping controllers will be detailed. The concept of the BSC approach is to select suitable Lyapunov functions based on the control purposes of diverse design steps of the overall control system [23] - [25]. In this work, the Lyapunov functions selected for the DC-bus voltage and input current control can ensure tracking-errors converge to zero and overall system asymptotic stability.

4.1 Proposed BSC for DC-bus voltage loop

The main purposes that should be accomplished by regulating the DC-bus voltage involve leading V_{dc} to its desired reference (V_{dc}^*) in order to make its tracking error z_{dc} converges to zero asymptotically and to exactly provide the suitable d-axis input current reference (i_{fd}^*) utilized in the d-axis input current loop. The tracking error z_{dc} is given by:

$$z_{dc} = V_{dc} - V_{dc}^* \quad (18)$$

The dynamic of tracking error \dot{z}_{dc} is given by:

$$\dot{z}_{dc} = \dot{V}_{dc} - \dot{V}_{dc}^* \quad (19)$$

The first Lyapunov function selected in the DC-bus voltage loop V_1 and its dynamic \dot{V}_1 are given as:

$$\begin{cases} V_1 = \frac{1}{2} z_{dc}^2 \\ \dot{V}_1 = z_{dc} \dot{z}_{dc} \end{cases} \quad (20)$$

Using (19) and \dot{V}_{dc} given in (5), the dynamic of the first Lyapunov function \dot{V}_1 given in (20) becomes:

$$\dot{V}_1 = z_{dc} \left(\frac{v_{gd}}{C_{dc} V_{dc}} i_{fd} - \frac{V_{dc}}{C_{dc} R_L} - \dot{V}_{dc}^* \right) \quad (21)$$

To ensure the stability of the DC-bus voltage control loop, the term $\left(\frac{v_{gd}}{C_{dc} V_{dc}} i_{fd} - \frac{V_{dc}}{C_{dc} R_L} - \dot{V}_{dc}^* \right)$ must be expressed as:

$$\frac{v_{gd}}{C_{dc} V_{dc}} i_{fd} - \frac{V_{dc}}{C_{dc} R_L} - \dot{V}_{dc}^* = -k_{dc} z_{dc} \quad (22)$$

where, k_{dc} is a positive constant and i_{fd}^* is the d-axis input current reference that stabilize the DC-bus voltage.

From (22), the virtual command $u_{dc} = i_{fd}^*$ of the DC-bus voltage loop is given by:

$$i_{fd}^* = \frac{C_{dc} V_{dc}}{v_{gd}} \left(-k_{dc} z_{dc} + \frac{V_{dc}}{C_{dc} R_L} + \dot{V}_{dc}^* \right) \quad (23)$$

4.2 Proposed BSC for input currents loops

The objective is to obtain dq0-axes input voltage references v_{fdq0}^* with zero transient and steady-state errors. This can be achieved mainly through forcing the dq0-axes input currents i_{fdq0} to track their references i_{fdq0}^* to make their tracking-errors converge to zero. The tracking-errors of the input currents z_{dq0} are given by:

$$\begin{cases} z_d = i_{fd} - i_{fd}^* \\ z_q = i_{fq} - i_{fq}^* \\ z_0 = i_{f0} - i_{f0}^* \end{cases} \quad (24)$$

The dynamics of these tracking-errors \dot{z}_{dq0} can be expressed as:

$$\begin{cases} \dot{z}_d = \dot{i}_{fd} - \dot{i}_{fd}^* \\ \dot{z}_q = \dot{i}_{fq} - \dot{i}_{fq}^* \\ \dot{z}_0 = \dot{i}_{f0} - \dot{i}_{f0}^* \end{cases} \quad (25)$$

The three adopted Lyapunov functions are defined as $V_{dq0} = \frac{1}{2} z_{dq0}^2$, and their derivatives can be expressed as:

$$\begin{cases} \dot{V}_d = z_d \dot{z}_d \\ \dot{V}_q = z_q \dot{z}_q \\ \dot{V}_0 = z_0 \dot{z}_0 \end{cases} \quad (26)$$

By substituting the dynamics \dot{i}_{fdq0} from (6) into (25), it results:

$$\begin{cases} \dot{V}_d = z_d \left(\frac{1}{L_f} u_d - \frac{R_f}{L_f} i_{fd} - \dot{i}_{fd}^* \right) \\ \dot{V}_q = z_q \left(\frac{1}{L_f} u_q - \frac{R_f}{L_f} i_{fq} - \dot{i}_{fq}^* \right) \\ \dot{V}_0 = z_0 \left(\frac{1}{(L_f + 3L_n)} u_0 - \frac{(R_f + 3R_n)}{(L_f + 3L_n)} i_{f0} - \dot{i}_{f0}^* \right) \end{cases} \quad (27)$$

In order to guarantee the stability of the dq0-axes input currents controllers, the time derivative of the three Lyapunov functions in system Eqs. (26) must be strictly negative. For this, the three terms $\left(\frac{1}{L_f} u_d - \frac{R_f}{L_f} i_{fd} - \dot{i}_{fd}^* \right)$, $\left(\frac{1}{L_f} u_q - \frac{R_f}{L_f} i_{fq} - \dot{i}_{fq}^* \right)$, and $\left(\frac{1}{(L_f + 3L_n)} u_0 - \frac{(R_f + 3R_n)}{(L_f + 3L_n)} i_{f0} - \dot{i}_{f0}^* \right)$ must be expressed as:

$$\begin{cases} \frac{1}{L_f} u_d - \frac{R_f}{L_f} i_{fd} - \dot{i}_{fd}^* = -k_d z_d \\ \frac{1}{L_f} u_q - \frac{R_f}{L_f} i_{fq} - \dot{i}_{fq}^* = -k_q z_q \\ \frac{1}{(L_f + 3L_n)} u_0 - \frac{(R_f + 3R_n)}{(L_f + 3L_n)} i_{f0} - \dot{i}_{f0}^* = -k_0 z_0 \end{cases}, \quad (28)$$

where, k_d , k_q , and k_0 are positive constants. Using (26) and (27), \dot{V}_{dq0} given by system Eqs. (26) become:

$$\begin{cases} \dot{V}_d = -k_d z_d^2 \\ \dot{V}_q = -k_q z_q^2 \\ \dot{V}_0 = -k_0 z_0^2 \end{cases}. \quad (29)$$

As can be seen from (29), it is clear that the dynamics of the three Lyapunov functions \dot{V}_d , \dot{V}_q , and \dot{V}_0 are strictly negative. It means that the tracking-errors z_d , z_q , and z_0 will converge to zero. Thus, the stability of the dq0-axes input currents controllers can be ensured. According to (28), the decoupling control variables u_d , u_q , and u_0 of the dq0-axes input currents loops are computed as:

$$\begin{cases} u_d = L_f (-k_d z_d + \frac{R_f}{L_f} i_{fd} + \dot{i}_{fd}^*) \\ u_q = L_f (-k_q z_q + \frac{R_f}{L_f} i_{fq} + \dot{i}_{fq}^*) \\ u_0 = (L_f + 3L_n) (-k_0 z_0 + \frac{R_f + 3R_n}{L_f + 3L_n} i_{f0} + \dot{i}_{f0}^*) \end{cases}. \quad (30)$$

By using the system Eq. (7), the dq0-axes four-leg rectifier input voltage references v_{fdq0}^* can be expressed as:

$$\begin{cases} v_{fd}^* = -L_f (-k_d z_d + \frac{R_f}{L_f} i_{fd} + \dot{i}_{fd}^*) + L_f \omega i_{fq} + v_{gd} \\ v_{fq}^* = -L_f (-k_q z_q + \frac{R_f}{L_f} i_{fq} + \dot{i}_{fq}^*) - L_f \omega i_{fd} \\ v_{f0}^* = -(L_f + 3L_n) (-k_0 z_0 + \frac{R_f + 3R_n}{L_f + 3L_n} i_{f0} + \dot{i}_{f0}^*) \end{cases}, \quad (31)$$

where k_{dc} and k_{dq0} are positive constants, which are chosen as $k_{dc}=320$ and $k_{dq0}=10^6$.

These parameters are selected so that the input current control loop's dynamics must be faster than the DC-bus voltage control loop's dynamics and to achieve good control performance while considering the system stability, robustness, and dynamic response.

Without using Park transformation, the input voltage references $v_{f\alpha\beta 0}^*$ in the $\alpha\beta 0$ -frame required by the 3DSVPWM method can be provided from the input voltage references in the dq0-frame v_{fdq0}^* given by (31) using (17) as follows:

$$\begin{bmatrix} v_{f\alpha}^* \\ v_{f\beta}^* \\ v_{f0}^* \end{bmatrix} = \frac{1}{V_{gmax}} \begin{bmatrix} v_{g\alpha} & v_{g\beta} & 0 \\ v_{g\beta} & -v_{g\alpha} & 0 \\ 0 & 0 & 1 \end{bmatrix} \begin{bmatrix} v_{fd}^* \\ v_{fq}^* \\ v_{f0}^* \end{bmatrix}. \quad (32)$$

On the other hand, the output control variables of the PICs used in the DC bus voltage and input current loops for achieving the comparative with the proposed BSC are given as follows:

$$i_{fd}^* = (V_{dc}^* - V_{dc}) \left(k_{pdc} + \frac{k_{idc}}{s} \right), \quad (33)$$

$$v_{fd}^* = (i_{fdq0}^* - i_{fd0}) \left(k_{pdq0} + \frac{k_{idq0}}{s} \right), \quad (34)$$

k_p and k_i are the gains of the PICs, which are calculated using the pole placement method as follows:

$$\begin{cases} k_{pdq} = 2L_f \zeta_i \omega_{ni} - R_f \\ k_{idq} = L_f \omega_{ni}^2 \\ k_{pdq} = 2(L_f + 3L_n) \zeta_i \omega_{ni} - (R_f + 3R_n) \\ k_{i0} = (L_f + 3L_n) \omega_{ni}^2 \end{cases} \quad (35)$$

$$\begin{cases} k_{pdc} = 2C_{dc} \zeta_{dc} \omega_{ndc} \\ k_{idc} = C_{dc} \omega_{ndc}^2 \end{cases}, \quad (36)$$

where ω_n and ζ are the natural-frequency and damping factor of PICs, respectively. ζ_{dc} and ζ_i are sets to 0.707 for suitable overshoot under a transient process of both control loops, and ω_{ndc} and ω_{ni} are sets respectively to 60 and 3×10^3 rad/s.

5 Experimental Validation

Fig. 3 illustrates the setup of PIL co-simulation for the four-leg rectifier connected to the three-phase four-wire grid shown in Fig. 1. The control is performed using the DSP card STM32F407 discovery board. The details on how this DSP card was used to create PIL co-simulation are discussed in [29] and [30].

To confirm and validate the viability and effectiveness of the proposed VOC-DPC with BSC in enhancing the control performance and dynamic responses of the four-leg rectifier, comparative PIL co-simulation results between the suggested BSC and traditional PI control are presented. The system parameters used in the PIL co-simulation are presented in Table 1.

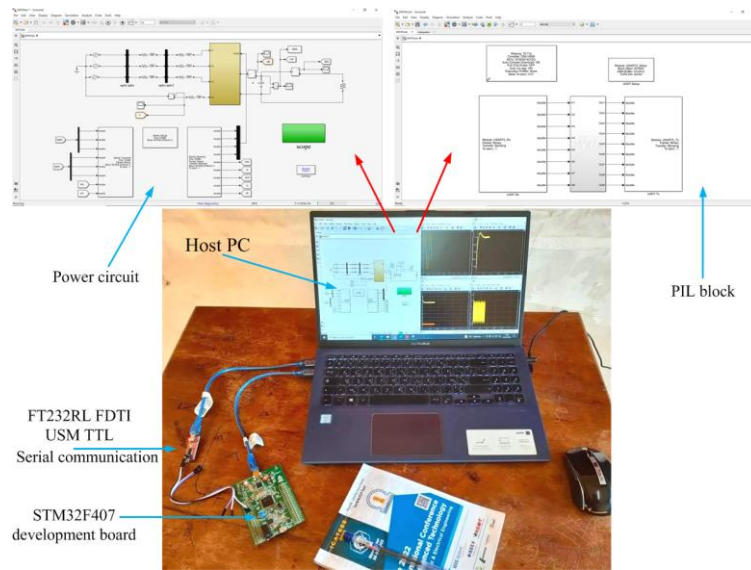


Figure 3. STM development board for processor-in-the-loop validation of the proposed control method.

Table 1. System parameters.

Parameter	Value
AC grid voltage V_{gmax}	120 V
Grid voltage frequency	50 Hz
DC-bus voltage V_{dc}	300 V
Capacitor of rectifier DC side C_{dc}	840 μ F
DC load resistance R_L	100 Ω
Input filter inductances L_f, L_{fn}	10 mH, 5 mH
Input filter resistances R_f, R_{fn}	0.3 Ω
Grid inductances L_g, L_{gn}	0.1 mH, 0.05 mH
Grid resistances R_g, R_{gn}	0.1 Ω

In order to get precise information about the dynamic performances, the control performance the analysis of the control performance was first performed at the nominal values of the load and the DC bus voltage. Furthermore, in this case, the robustness of the two control strategies was evaluated with variations of the filter inductance, when the filter inductance varied from 1 to 3 mH. The response time, DC-bus voltage stabilization and oscillations, reactive power compensation, input current harmonics and zero-sequence elimination, and neutral current oscillation reduction using the proposed BSC and traditional PI control were then evaluated under diverse conditions, including load and DC-bus voltage variations. The comparative study of PIL co-simulation results between the proposed BSC and the traditional PI control are shown in Figures. 4–8.

First, the steady-state control performance of the DC-bus voltage and input current and their tracking errors and oscillations using both control techniques are shown in Figure. 4 (a and b). The curves from top to bottom in these figures are the DC-bus voltage, dq-axes input currents, zero-sequence input current, and first-phase input current and its corresponding grid voltage. These figures confirm that both control techniques used in the VOC-DPC method achieve constant DC-bus voltage and unit power factor, but the proposed BSC significantly reduces tracking errors and oscillations in the DC-bus voltage and input currents compared to traditional PI control.

The harmonic spectra of the input current for the two control techniques at the nominal value of the filter inductance are shown in Fig. 5(a and b). The total harmonic distortion (THD) is also significantly reduced using the suggested BSC compared to the traditional PI. Indeed, the THD was lowered from 3.18% using PI to 0.59% using the BSC.

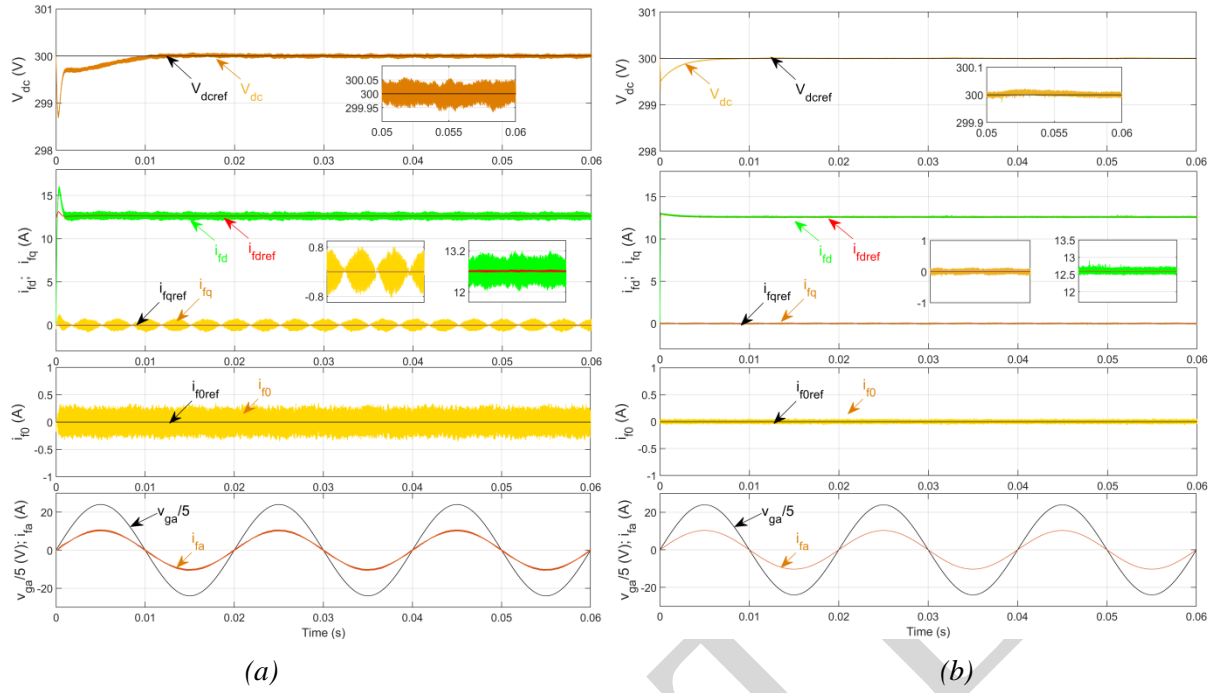


Figure 4. Steady-state responses of the proposed VOC-DPC method: (a) traditional PI control and (b) proposed BSC.

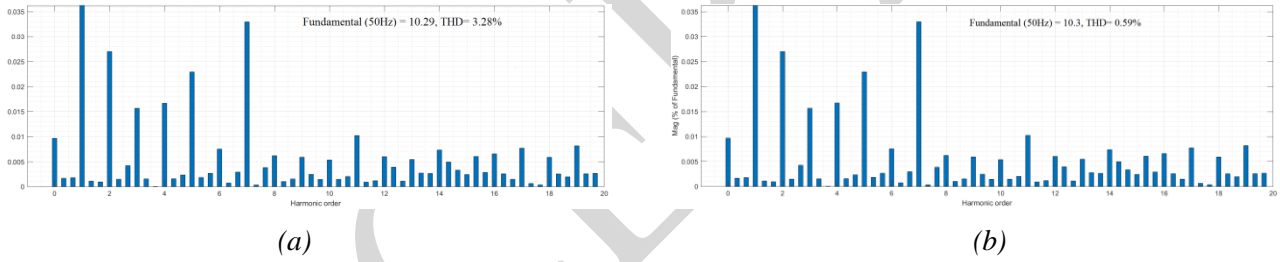


Figure 5. Harmonic spectrum of input current for: (a) traditional PI control and (b) proposed BSC.

Figure 6 illustrates the robustness performance of traditional PI and the proposed BSC when the filter inductance value L_f is varied from 0.5 to 3.5 mH. The figure clearly shows that the all-input current THD values obtained using the proposed BSC are lower than those of the traditional PI control for all filter inductance values. This confirms the robustness of the proposed BSC against the filter inductance variations.

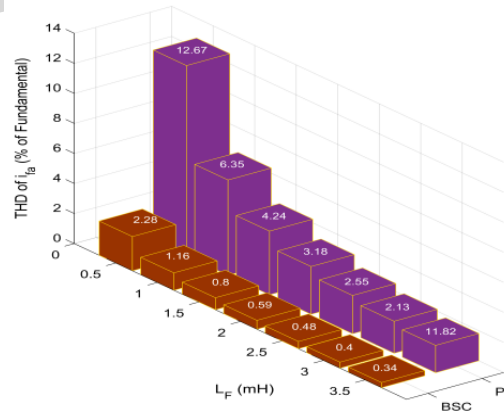


Figure 6. Input currents THDs versus filter inductor variation using both control techniques.

Another set of PIL co-simulation tests is performed with the aim to compare transient dynamic responses and control performance of the DC-bus voltage and input currents using both control techniques under DC-bus voltage and load variations.

Figures 7 and 8 (a and b) compare the transient dynamic responses and control performance of the VOC-DPC method based on traditional PI and the proposed BSC when the reference of the DC-bus voltage is changed from 300 to 320 V at 0.06 s. The curves from top to bottom in figure 8 (a and b) are the d-axis input current, q-axis input current, zero-sequence input current, and first-phase input current and its corresponding grid voltage. It can be seen from these figures that the transient response, tracking errors, and oscillations of the DC-bus voltage and input currents under DC-bus voltage change are much better when the proposed BSC is used compared with traditional PI control. When the DC-bus voltage is step changed, the DC-bus voltage tracks its new reference value (320 V) very quickly in just 8 ms without any overshoot in the case of the proposed BSC compared to the traditional PI, which has a large response time and voltage-overshoot.

After the change in DC-bus voltage, it is easy to see that the suggested BSC achieves faster dynamic responses and better steady state performance than the traditional PI. The d-axis input current i_{fd} tracks its new reference value (14 A) in 6 ms, with lower current draw in the proposed BSC case compared to the PI (the d-axis input current draw at this change is 27 A in the case of the PI controller, while the proposed BSC results in only 10 A). It should be noted here that the curve of d-axis input current reference i_{fd}^* is different in the two control techniques because it is provided by the DC-bus voltage control loop. After this change and during the steady state, the d-axis input current i_{fd} stays around at its new reference (46.5 A), and the q0-axes input currents i_{fq} and i_{f0} are not influenced by this change and stay around 0 A with very small oscillations using the proposed BSC, which perfectly reduces the neutral grid current oscillation and ensures decoupling control and unity power factor, as shown in the curve of first-phase input current and its corresponding grid voltage.

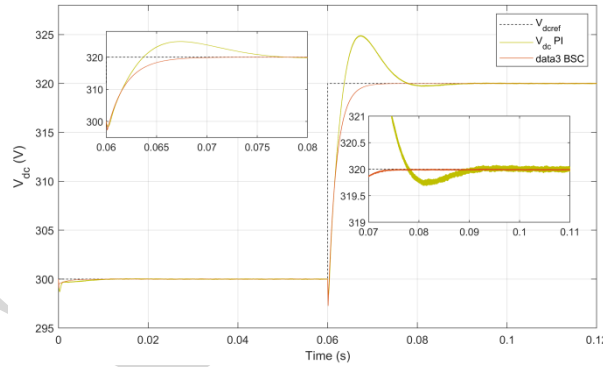


Figure 7. Transient response and performance of the DC-bus voltage under DC-bus voltage change from 300 to 320 V at 0.06 s.

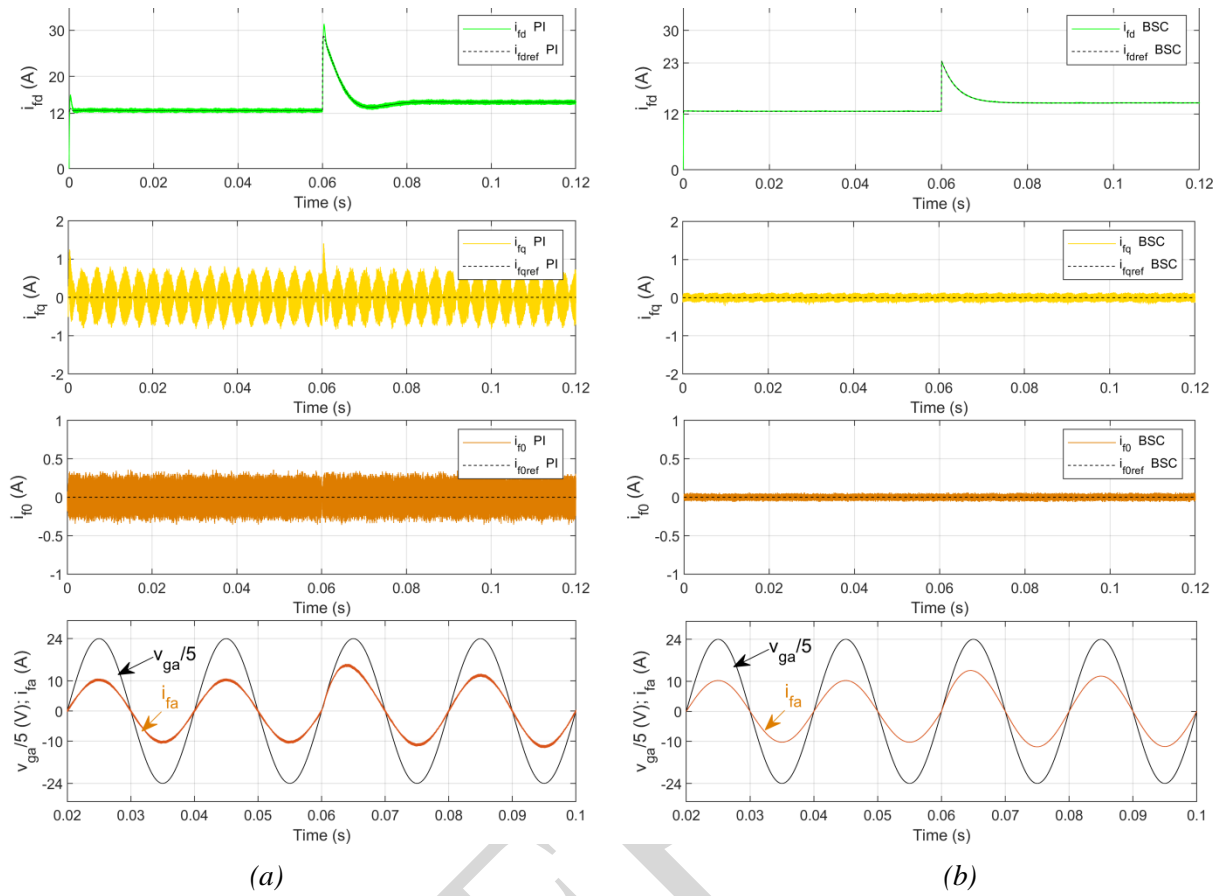


Figure 8. Transient response and performance of the input currents under DC-bus voltage change from 300 to 320 V at 0.06 s.

Figs. 9 and 10 (a and b) compare the transient responses and control performance of the VOC-DPC method based on the traditional PI and proposed BSC when the load is changed from 50 to 25 Ω at 0.06 s.

As shown in Fig. 10, using the traditional PI controller, a significant voltage drop appears in the DC-bus voltage at the change of the load before returning to its reference value with a long settling time of nearly 0.08s. In contrast, when the proposed BSC is used, the DC-bus voltage response is relatively fast and returns to its reference value in just 5 ms with a low amount of voltage drop, offering fast dynamic response. Additionally, the oscillation before and after the load change is significantly less in the case of the suggested BSC.

When the suggested BSC is used, the dq0-axes input currents follow their references with very small oscillations even when the load changes, as shown in Figs. (a) and 10(b). The d-axis input current changes according to the load and follows its new reference value provided by the DC-bus voltage control loop very quickly with a very low current draw, while the q0-axes input currents continue to oscillate around zero and are unaffected by this change, ensuring perfect decoupling control. As can also be seen, the first-phase input current and its corresponding grid voltage are in phase, providing a unity power factor, as desired. The input current has very low ripple when the suggested BSC is applied.

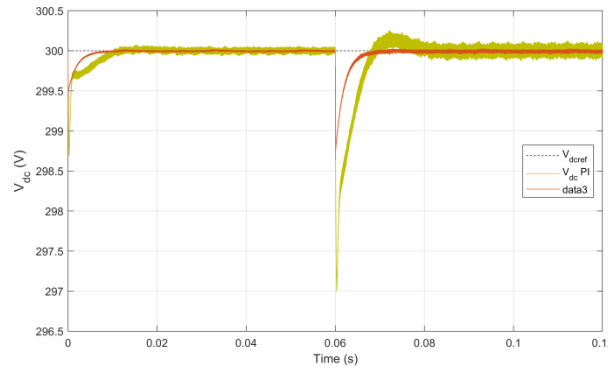


Figure 9. Transient response and control performance of the DC-bus voltage under load change from 50 to 25 Ω at 0.06 s.

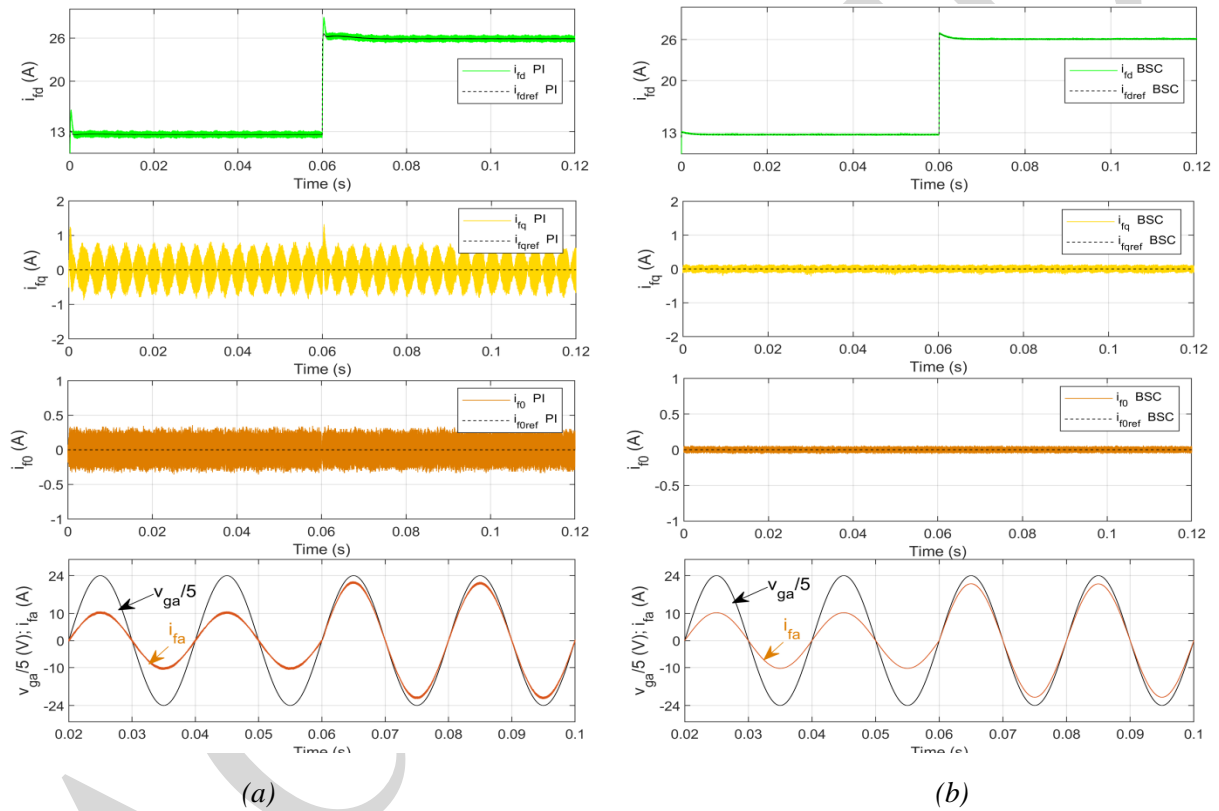


Figure 10. Transient response and performance of the input currents under load change from 50 to 25 Ω at 0.06 s.

6 Conclusions

In this paper, a combined method for voltage-oriented control and direct power control (VOC-DPC) in conjunction with backstepping control technique in synchronous rotating field is proposed for a three-phase four-wire rectifier with grid connection without phase-locked loop (PLL) and park transformation, to achieve DC-link voltage stabilization and control, high power factor, low grid current harmonics, low zero-sequence current oscillations, perfect decoupling input current control, high robustness against filter inductance variations, low computational burden, and better transient responses under DC-bus voltage and load. The suggested BSC employs four separate backstepping controllers designed based on Lyapunov theory to simultaneously regulate DC voltage and input currents.

The proposed VOC-DPC method associated with the backstepping control technique is validated in a wide range of tests through PIL co-simulation combined with MATLAB/Simulink. Moreover, the backstepping based VOC-DPC method has been compared to the traditional PI controller. The result is that backstepping

improves the control performance and dynamic behavior in two ways: first, the proposed backstepping method for the rectifier DC -bus voltage control loop achieves much lower response time, overshoot, tracking error and oscillation than the traditional PI -method, and the transient response is significantly reduced when the DC -bus voltage and load are changed; second, the proposed backstepping method for the rectifier input current control loops achieves faster response and very low tracking error performance, perfect decoupling control, very low current consumption and oscillation, while providing lower input current harmonic and zero current ripple. In addition, backstepping control shows greater robustness to parameter variations than the traditional PI controller.

References

- [1] Mandrioli, R., Viatkin, A., Hammami, M., Ricco, M., & Grandi, G., "A comprehensive AC current ripple analysis and performance enhancement via discontinuous PWM in three-phase four-leg grid-connected inverters. *Energies*, vol. 13, no. 17, pp. 4352, 2020, doi:10.3390/en13174352.
- [2] Olives-Camps, J. C., Mauricio, J. M., Barragán-Villarejo, M., & Matas-Díaz, F. J., "Voltage control of four-leg VSC for power system applications with nonlinear and unbalanced loads," *IEEE Trans. Energy Convers.*, vol. 35, no. 2, pp. 640-650, 2019, doi:10.1109/TEC.2019.2957185.
- [3] Jiao, S., Potti, K. R. R., Rajashekara, K., & Pramanick, S. K., "A novel DROGI-based detection scheme for power quality improvement using four-leg converter under unbalanced loads," *IEEE Trans. Ind. Applicat.*, vol. 56, no. 1, pp. 815-825, 2019, doi:10.1109/TIA.2019.2942798.
- [4] Viatkin, A., Hammami, M., Grandi, G., & Ricco, M., "Analysis of a Three-Phase Four-Leg Front-End Converter for EV Chargers with Balanced and Unbalanced Grid Currents," in *Proc. of the 2019 45th Ann. Conf. IEEE Ind. Electronic. Society, IECON 2019, 14-17 October 2019, Lisbon, Portugal* vol. 1, pp. 3442-3449, doi:10.1109/IECON.2019.8926791.
- [5] Chebabhi, A., Fellah, M. K., Kessal, A., & Benkhoris, M. F., "Comparative study of reference currents and DC-bus voltage control for three-phase four-wire four-leg SAPF to compensate harmonics and reactive power with 3D SVM," *ISA transactions*, vol. 57, pp. 360-372, 2015, doi:10.1016/j.isatra.2015.01.011.
- [6] Dheepanchakkravarthy, A., Akhil, S., Venkatraman, K., Selvan, M. P., & Moorthi, S., "Performance analysis of FPGA controlled four-leg DSTATCOM for multifarious load compensation in electric distribution system," *Engineering science and technology, an international journal*, vol. 21, no. 4, pp. 692-703, 2018, doi:10.1016/j.jestch.2018.05.004.
- [7] Li, A., Jiang, D., Kong, W., & Qu, R., "Four-leg converter for reluctance machine with dc-biased sinusoidal winding current," *IEEE Trans. Power Electron.*, vol. 34, no. 5, pp. 4569-4580, 2018, doi:10.1109/TPEL.2018.2864244.
- [8] Viatkin, A., Mandrioli, R., Hammami, M., Ricco, M., & Grandi, G., "AC Current Ripple Harmonic Pollution in Three-Phase Four-Leg Active Front-End AC/DC Converter for On-Board EV Chargers," *Electronics*, vol. 10, no. 2, pp. 116, 2021, doi: 10.3390/electronics10020116.
- [9] Chebabhi, A., Abdelhalim, K., Fellah, F. M. K., & Fayssal, A., "Self tuning filter and fuzzy logic control of shunt active power filter for eliminates the current harmonics constraints under unbalanced source voltages and loads conditions," *Journal of Power Technologies*, vol. 98, no. 1, pp. 1-19, 2018, papers.itc.pw.edu.pl/index.php/JPT/article/view/1120.
- [10] Nian, H., Cheng, P., Zhu, Z. Q., "Coordinated Direct Power Control of DFIG System Without Phase-Locked Loop Under Unbalanced Grid Voltage Conditions," *IEEE Trans. Power Electron.*, vol. 31, no. 4, pp. 2905-2918, 2016, doi:10.1109/TPEL.2018.2864244.
- [11] Ali, Z., Christofides, N., Hadjidemetriou, L., Kyriakides, E., Yang, Y., & Blaabjerg, F., "Three-phase phase-locked loop synchronization algorithms for grid-connected renewable energy systems: A review," *Renewable and Sustainable Energy Reviews*, vol. 90, pp. 434-452, 2018, doi:10.1016/j.rser.2018.03.086.
- [12] Song, Y., & Blaabjerg, F., "Analysis of middle frequency resonance in DFIG system considering phase-locked loop," *IEEE Trans. Power Electron.*, vol. 33, no. 1, pp. 343-356, 2017, doi:10.1109/TPEL.2017.2672867.
- [13] H. Nian, P. Cheng, and Z. Q. Zhu., "Coordinated direct power control of DFIG system without phase-locked loop under unbalanced grid voltage conditions," *IEEE Trans. Power Electron.*, vol. 31, no. 4, pp. 2905-2918, 2016, doi:10.1109/TPEL.2015.2453127.
- [14] Din, Z., Zhang, J., Bassi, H., Rawa, M., & Song, Y., "Impact of phase locked loop with different types and control dynamics on resonance of DFIG system," *Energies*, vol. 13, no. 5, pp. 1039, 2020,

doi:10.3390/en13051039.

- [15] Gui, Y., Xu, Q., Blaabjerg, F., & Gong, H., "Sliding mode control with grid voltage modulated DPC for voltage source inverters under distorted grid voltage," *CPSS Transactions on Power Electronics and Applications*, vol. 4, no. 3, pp. 244-254, 2019, doi:10.24295/CPSSSTPEA.2019.00023.
- [16] Cheng, P., Wu, C., Ning, F., & He, J., "Voltage modulated DPC strategy of DFIG using extended power theory under unbalanced grid voltage conditions," *Energies*, vol. 13, no. 22, pp. 6077, 2020, doi:10.3390/en13226077.
- [17] Alqatamin, M., Latham, J., Smith, Z. T., "Grainger, B. M., & McIntyre, M. L., "Current control of a three-phase, grid-connected inverter in the presence of unknown grid parameters without a phase-locked loop," *IEEE J. Emer. Selec. Top. Power Electron.*, vol. 9, no. 3, pp. 3127-3136, 2020, doi:10.1109/JESTPE.2020.3001153.
- [18] Pichan, M., & Rastegar, H., "Sliding-mode control of four-leg inverter with fixed switching frequency for uninterruptible power supply applications," *IEEE Trans. Ind. Electron.*, vol. 64, no. 8, pp. 6805-6814, 2017, doi:10.1109/TIE.2017.2686346.
- [19] Lokesh, N., & Mishra, M. K., "Design of a decoupled sliding mode control for four-leg distribution static compensator," *IEEE Trans. Pow. Del.*, vol. 37, no. 6, pp. 5014-5024, 2022, doi:10.1109/TPWRD.2022.3165942.
- [20] Fahmy, A. M., et al, "A four leg shunt active power filter predictive fuzzy logic controller for low-voltage unbalanced-load distribution networks," *Journal of Power Electronics* vol. 18, no. 2, pp. 573-587, 2018, doi:10.6113/JPE.2018.18.2.573.
- [21] Chebabhi, A., Fellah, M. K., Kessal, A., & Benkhoris, M. F., "A new balancing three level three dimensional space vector modulation strategy for three level neutral point clamped four leg inverter based shunt active power filter controlling by nonlinear back stepping controllers," *ISA transactions*, vol. 63, pp. 328-342, 2016, doi:10.1016/j.isatra.2016.03.001.
- [22] Badra, M. S., Barkat, S., & Bouzidi, M., "Backstepping control of three-phase three-level four-leg shunt active power filter," *Journal of Fundamental and Applied Sciences*, vol. 9, no. 1, pp. 274-307, 2017, doi:10.4314/jfas.v9i1.18.
- [23] Sun, D., Wang, X., & Fang, Y., "Backstepping direct power control without phase-locked loop of AC/DC converter under both balanced and unbalanced grid conditions," *IET Power Electronics*, vol. 9, no. 8, pp. 1614-1624, 2016, doi:10.1049/iet-pel.2015.0653.
- [24] Wang, X., Sun, D., & Zhu, Z. Q., "Resonant-based backstepping direct power control strategy for DFIG under both balanced and unbalanced grid conditions," *IEEE Trans. Ind. Appl.*, vol. 53, no. 5, pp. 4821-4830, 2017, doi:10.1109/TIA.2017.2700280.
- [25] Li, J., Liu, Z., & Su, Q., "Improved adaptive backstepping sliding mode control for a three-phase PWM AC-DC converter," *IET Control Theory & Applications*, vol. 13, no. 6, pp. 854-860, 2019, doi:10.1049/iet-cta.2018.5453.
- [26] Wai, R. J., & Yang, Y., "Design of backstepping direct power control for three-phase PWM rectifier," *IEEE Trans. Ind. Appl.*, vol. 55, no. 3, pp. 3160-3173, 2019, doi:10.1109/TIA.2019.2893832.
- [27] Peng, F. Z., Lai, J.S., "Generalized instantaneous reactive power theory for three-phase power systems," *IEEE Trans. Instrum. Meas.*, vol. 45, no. 1, pp. 293-297, 1996, doi:10.1109/19.481350.
- [28] Zhu, S., & Hu, B., "Key technologies of active power filter for aircraft: a review," *Engineering Review*, vol. 36 no. 3, pp. 221-237, 2016, er.riteh.hr/index.php/ER/article/view/686.
- [29] Faddel, S., Saad, A. A., El Hariri, M., & Mohammed, O. A., "Coordination of hybrid energy storage for ship power systems with pulsed loads," *IEEE Trans. Ind. Appl.*, vol. 56, no. 2, pp. 1136-1145, 2019, doi:10.1109/TIA.2019.2958293.
- [30] Youcefa, B. E., Massoum, A., Barkat, S., & Wira, P., "Backstepping predictive direct power control of grid-connected photovoltaic system considering power quality issue," *Majlesi Journal of Electrical Engineering*, vol. 14, no. 1, pp. 9-23, 2020, <http://mjee.iaumajlesi.ac.ir/index/index.php/ee/article/view/2968>.